Virology 394 (2009) 276–285

Contents lists available at ScienceDirect

Virology

journal homepage: www.elsevier.com/locate/yviro

Molecular characterization of human parvovirus B19 genotypes 2 and 3

Zhaojun Chen [a,b], Wuxiang Guan [b], Fang Cheng [b], Aaron Yun Chen [b], Jianming Qiu [b,*]

[a] Department of Clinical Laboratory, The Affiliated Hospital of Hangzhou Normal University, Hangzhou, Zhejiang Province, China 310015
[b] Department of Microbiology, Molecular Genetics and Immunology, University of Kansas Medical Center, Mail Stop 3029, 3901 Rainbow Blvd., Kansas City, KS 66160, USA

ARTICLE INFO

Article history:
Received 8 June 2009
Returned to author for revision 28 July 2009
Accepted 26 August 2009
Available online 15 September 2009

Keywords:
Parvovirus
B19
Genotype
Transcription
Replication
Apoptosis

ABSTRACT

We have characterized the transcription profiles of parvovirus B19 (B19V) genotype-2 A6 and genotype-3 V9 variants. The A6 RNA profile differs from that of the prototype B19V in both B19V non-permissive and permissive cells, whereas the overall profile of the V9 RNA in these cells is similar to that of the prototype. A unique feature we have identified is that the genotype-2 A6 variant used only one splice acceptor to remove the first intron. We also demonstrated that the inverted terminal repeats (ITRs) of the prototype B19V support replication of the V9 genome, which produces infectious virus, but not that of the A6 genome, in B19V-permissive cells. Similar to the proapoptotic nature of the prototype B19V large non-structural protein (NS1), the A6 and V9 NS1 proteins also are potent inducers of apoptosis in B19V-permissive cells.

Introduction

Human parvovirus B19 (B19V) is the only parvovirus that has been confirmed to be pathogenic in humans until the discovery of human bocavirus (Allander et al., 2005). B19V causes a variety of diseases, including erythema infectiosum (fifth disease) in children, acute or chronic arthropathy in adults, aplastic crisis in patients with chronic hemolytic anemia, persistent anemia in immunodeficient and immunocompromised patients, and fetal hydrops in pregnant women (Young and Brown, 2004). Recently a number of B19V variants were reported to vary extensively from the prototype B19V with respect to genomic sequence, exhibiting greater than 12% divergence versus the less than 2% divergence characteristic of previously characterized prototype B19V isolates (Servant et al., 2002; Hokynar et al., 2002; Nguyen et al., 1999). Of these, the V9 variant, which was isolated from a patient with aplastic crisis, diverged by about 12% sequence from prototype B19V isolates (Nguyen et al., 1999). The A6 variant, which was isolated from an anemic HIV-positive patient, exhibited 12% divergence from the prototype B19V, and 8% divergence from the V9 variant (Nguyen et al., 2002). The sequences of other reported A6-related isolates, including the LaLi isolate, were 98% identical to that of the A6 variant (Hokynar et al., 2002). Therefore, the human erythrovirus is now classified into three distinct genotypes (Servant et al., 2002). Genotype-1 is composed of all the prototype B19V isolates, genotype-2 includes the A6, LaLi and their related isolates (Blumel et al., 2005; Norja et al., 2006; Sanabani et al., 2006), and genotype-3 comprises the V9 and V9-related isolates (Sanabani et al., 2006; Candotti et al., 2004).

The B19V genome contains two identical terminal repeats (ITRs) of approximately 380 nucleotides; these are imperfect palindromes and form hairpin loops. However, the terminal repeats of genotype-2 and genotype-3 have not been cloned and sequenced. The genotype-1 replicates restrictively in the erythroid progenitors of human bone marrow, often producing exceptionally high numbers of progeny virus in the blood (Ozawa et al., 1986; Srivastava and Lu, 1988). In contrast, high virus-load viremias of genotype-2 and genotype-3 have been identified only occasionally (Blumel et al., 2005; Nguyen et al., 1999, 2002; Servant et al., 2002; Liefeldt et al., 2005). However, both of these genotypes have been associated with anemia or aplastic crisis, indicating their tropism for erythroid cells (Blumel et al., 2005; Nguyen et al., 1999; Sanabani et al., 2006; Candotti et al., 2004). Cross-reactivity of 100% in antibody activities among these three genotypes supports the notion that they comprise only a single serotype (Ekman et al., 2007). It is not yet known whether the variations among the genomes of human erythrovirus variants are responsible for their distinct biological and pathological properties. The P6 promoter activities of the three genotypes have been shown to be identical, to be most pronounced in B19V-permissive cells (Ekman et al., 2007). However, the overall transcriptional profiles of the B19V genotype-2 and genotype-3 and their replication competence with the genotype-1 ITRs have not been explored.

The disease outcome of B19V infection as seen in transient aplastic crisis, pure red cell aplasia and hydrops fetalis is due to the direct cytotoxicity of the virus to the erythroid progenitors that are native host of B19V replication (Brown and Young, 1997). It has been shown that during B19V infection of primary erythroid progenitor cells and

* Corresponding author. Fax: +1 913 588 7295.
E-mail address: jqiu@kumc.edu (J. Qiu).

0042-6822/$ – see front matter © 2009 Elsevier Inc. All rights reserved.
doi:10.1016/j.virol.2009.08.044

myeloid cell lines (Sol et al., 1999; Moffatt et al., 1998), e.g. UT7/Epo-S1, progressive apoptosis is induced. In UT7/Epo-S1 cells, this B19V-induced apoptosis has been shown to be associated with expression of the large non-structural protein (NS1) (Sol et al., 1999; Moffatt et al., 1998). The amino acid sequence of the A6 and V9 NS1 proteins diverge from that of the prototype-encoded counterpart by 6.2% and 6.1%, respectively. The potency of both NS1 proteins of the B19V genotypes 2 and 3 in inducing apoptosis has not yet been examined.

In the current study, we have used a replication competence system in COS-7 cells to systematically characterize the transcription profiles of the two B19V genotypes with the cloned nearly-fully length genome of the A6 (genotype-2) and V9 (genotype-3) variants. We also investigated the replication competence of the ITRs from the prototype B19V in the context of the V9 and A6 genomes. Finally, we evaluated the potency of the two novel NS1 proteins encoded by B19V genotypes 2 and 3 in inducing apoptosis in B19V-permissive cells.

Results

Transcriptional profiles of human erythroviruses V9 and A6

We and others previously showed that the B19V transcription profile in COS-7 cells transfected with an SV40 replication origin (SV40-ori)-containing B19V plasmid closely resembles to that from B19V-infected human bone marrow or erythroid progenitor cells (St et al., 1991; Guan et al., 2008). Therefore, in this study, we used SV40-ori-containing A6 and V9 plasmids (pC1V9 and pC1A6) to transfect COS-7 cells. Replications of these two plasmids in COS-7 cells were confirmed by Southern blot (data not shown). Transcription profiles were generated from total RNAs isolated from these cells, using RNase protection and Northern blot analysis.

RNase protection analysis of V9 (A6) RNA

Total RNA isolated from pC1V9- or pC1A6-transfected COS-7 cells was subjected to RNase protection using probes targeted to the promoters, intron donor and acceptor sites, and polyadenylation sites. The B19V genetic map was used as a guide.

V9 (A6) P1 probe

Protection with the V9 (A6) P1 probe, which spans the putative P6 promoter, yielded bands of approximately 192 (193) nts and 58 nts, respectively. The 192(193)-nt and 58-nt bands represent RNAs that were transcribed from the P6 promoter and were unspliced and spliced, respectively, at the first donor site (D1). Thus, the P6 RNA initiation site of V6 (A6) was located at approximately nt 242 (148), and the D1 donor site was confirmed to be at nt 298 (205). RNA spliced from the D1 donor site accumulated to levels approximately 10 times greater than that of RNA unspliced at the D1 site, in the cases of both the V9 and A6 RNAs (Fig. 1B and C, lane 1).

V9 (A6) P2 probe

Protection with the P2 probe, which covers the putative A1-1 and A1-2 acceptors and D2 donor sites, was predicted to yield five bands of 563 (561), 471 (472), 351 (352), 274 and 154 nts. The bands at 563 (561) nts, 471 (472) nts and 351 (352) nts, which protected both the V9 and A6 RNAs from transfected COS-7 cells (Figs. 1B and C, lane 2), represent RNAs that were unspliced and spliced at A1-1 and A1-2, respectively; these RNAs were all unspliced at the D2 donor site. The band at 274 nts represents RNA spliced from the A1-1 acceptor to the D2 donor, and was protected in both V9 and A6 RNA. These results confirmed the A1-1 acceptor and the D2 donor at nt 1802 (1709) and nt 2075 (1982), respectively.

Surprisingly, the 154-nt band that represents RNA spliced at A1-2 acceptor and at the D2 donor was protected in the V9 RNA, but not the A6 RNA (Figs. 1B and C, lane 2), indicating that the A1-2 acceptor may not be utilized significantly during the processing of A6 RNA isolated from transfected COS-7 cells. This result thus conformed the A1-2 acceptor of the V9 at nt 1922. To examine further the use of the A1-2 acceptor in processing of the A6 RNA in a B19V-permissive cell system, we transfected pC1A6 into UT7/Epo-S1 cells. Total RNA was protected with the A6 probe P2; however, a band at 154 nts, which represents RNA spliced at the A1-2 acceptor and D2 donor, and a band at 352 nts that represents RNA that is spliced at the A1-2 acceptor but not at the D2 donor were not protected (Fig. 1D, lane 2). In contrast, the corresponding bands were both protected in V9 RNA isolated from pC1V9-transfected UT7/Epo-S1 cells (Fig. 1D, lane 1). The 352-nt band protected in A6 RNA from COS-7 cells is likely non-specific degraded RNA (Fig. 1C, lane 2), as was confirmed repeatedly by RNase protection assays (data not shown). These results confirmed that the A1-2 acceptor was not significantly utilized in processing A6 RNAs produced in pC1A6-transfected COS-7 and UT7/Epo-S1 cells.

In cells transfected with pC1V9, the levels of RNA spliced at the A1-1 acceptor were approximately two-fold greater than those of the RNA spliced at the A1-2 acceptor, which is consistent with the findings for infection of erythroid progenitors with genotype-1 B19V (Guan et al., 2008).

V9 (A6) P3 probe

The P3 probe, which spans the two putative internal polyadenylation sites and the A2-1 acceptor, was protected to yield bands at approximately 665 (668) nts, 424 (423) nts, 159 (162) and 133 (124) nts (Figs. 1B and C, lane 3). The 665(668)-nt and 159(162)-nt bands represent RNAs unspliced and spliced at the A2-1 acceptor, respectively, which confirmed the A2-1 acceptor at nt 2937 (2844). The ratio of RNA that was spliced vs. unspliced at the A2-1 site was approximately 1:6. The 133(124)-nt and 424(423)-nt bands represent RNAs that were polyadenylated at the internal polyadenylation sites (pA)p1 and (pA)p2 sites, respectively, which identified the (pA)p1 and (pA)2 sites at nt 2562 (2461) and nt 2853 (2760), respectively. Apparently, about three times more RNA was polyadenylated at the (pA)p1 site.

V9 (A6) P4 and P5 probes

The P4 probe, which spans the A2-2 acceptor of the second intron, was protected to yield bands of approximately 243 (244) nts and 80 nts (Figs. 1B and C, lane 4), and these represent RNAs that were unspliced and spliced RNAs at the A2-2 acceptor site, respectively. This result confirmed the A2-2 acceptor site at nt 4596 (4503). The ratio of RNA that was spliced *vs* unspliced at the A2-2 was approximately 1:4. The P5 probe, which spans the distal polyadenylation site, was protected to yield mainly a single band of approximately 190 nts (Figs. 1B and C, lane 5). This indicates that the (pA)d cleavage site is at nt 4901 and nt 4808 for the V9 and A6, respectively.

Northern blot analysis of V9 and A6 RNA

Northern blot analysis of V9 RNA from COS-7 cells exhibited a pattern similar to that of the genotype-1 B19V (Beard et al., 1989; Liu et al., 2004). Hybridization of V9 RNA with the whole *NSCap* probe revealed four abundant RNA species that accumulated as bands of approximately 4.7 kb, 3.0/3.1 kb, 2.2/2.3 kb and 0.5-0.9 kb (Fig. 2, lane 2). These four bands were also detected following hybridization with the *Cap* probe (Fig. 2, lane 6), as well as with the *NS* probe (Fig. 2, lane 4), suggesting that all these RNA species were generated from a single promoter located upstream of the V9 genome. An RNA band of approximately 1.8 kb (indicated with an asterisk in Fig. 2, lanes 2, 4 and 6) was always hybridized with the three probes, and the nature of this band is unknown. Taken together, our findings indicate that the overall profile of V9 transcription is the same as that of genotype-1 B19V.

Hybridization of A6 RNA with the whole *NSCap* probe revealed four abundant RNA species similar to those from V9 RNA, i.e. 4.7 kb, 3.1 kb, 2.3 kb and 0.5–0.9 kb bands (Fig. 2, lane 3). These four bands were also detected following hybridization with the *Cap* probe (Fig. 2,

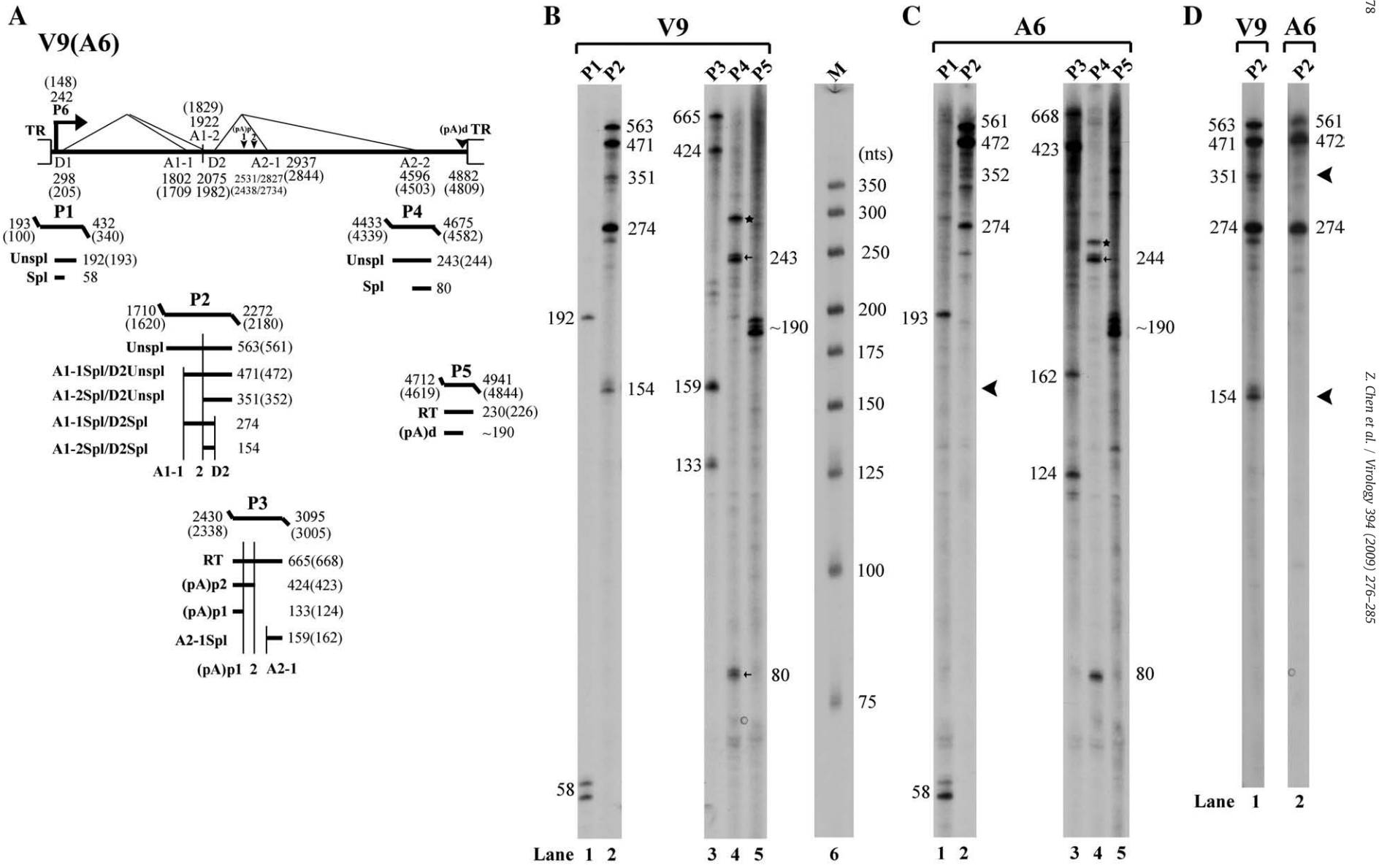

Fig. 1. Transcription mapping of V9 and A6 RNA by RNase protection assay (RPA). (A) Schematic diagram of the V9 (A6) genome and the probes used for RPA. The landmarks of transcription: the promoter (P6), the splice donor sites (D1 and D2), the acceptor sites (A1-1, A1-2, A2-1 and A2-2), the internal polyadenylation signal (pA)p and the distal polyadenylation sits (pA)d, are indicated. The RPA probes V9 (A6) P1, V9 (A6) P2, V9 (A6) P3, V9 (A6) P4 and V9 (A6) P5 are shown with their respective V9 nucleotide numbers with the A6 nucleotide numbers in parentheses, along with the designated bands they are expected to protect and their predicted sizes. Spl, spliced RNAs; Unspl, unspliced RNAs. (B and C) Mapping of the V9 (B) and A6 (C) transcription units by RPA. 10 μg of total RNA isolated two days after the transfection of COS-7 cells with plasmid pC1V9 (B) or pC1A6 (C) were protected by V9 (B) or A6 (C) probes P1, P2, P3, P4 and P5. Lane 1, ^{32}P-labeled RNA markers with sizes indicated. The sizes of the protected bands in the lanes are indicated. (D) RPA of V9 (A6) RNA isolated from transfected UT7/Epo-S1 cells. 10 μg of total RNA isolated two days after transfection of UT7/Epo-S1 cells with the plasmid pC1V9 or pC1A6 was protected by the V9 or A6 probe P2. The sizes of the protected bands in the lanes are indicated. Arrow heads indicate the absence of A6 RNAs spliced at the A1-2 site. Asterisks indicate undigested probe bands.

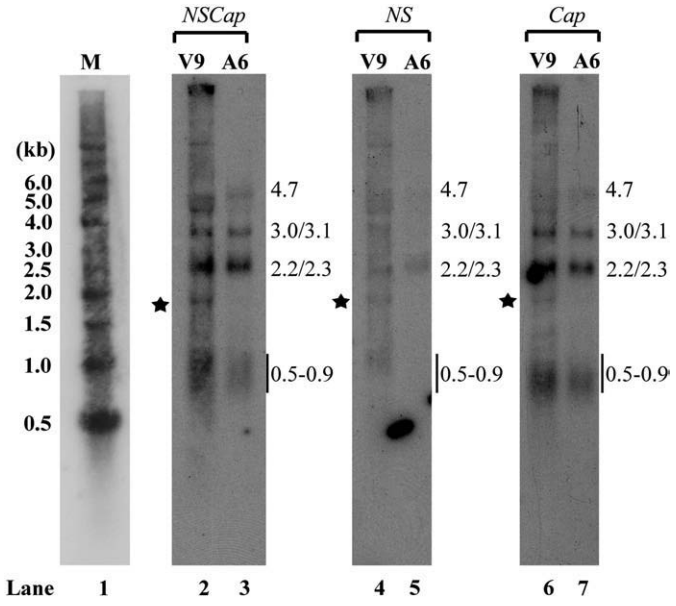

Fig. 2. Northern blot analysis of V9 and A6 RNA. Total RNA isolated from pC1V9- and pC1A6- transfected COS-7 cells 2 days post-transfection was used for Northern blot analysis. The blot was hybridized to three V9 DNA probes (*NSCap*, *NS* and *Cap*), which span various regions of the V9 genome, as indicated. The probes used are diagramed at the bottom of Fig. 3A. RNA bands detected by each probe are indicated by their respective sizes in kb to the right side of each blot. Asterisks indicate bands of unknown identity. RNA maker ladder (Ambion) is shown in lane 1.

lane 7). However, when it came to hybridization with the *NS* probe, unlike the V9 RNA, the A6 RNA did not produce small RNA bands at 0.5–0.9 kb. It is likely that the V9 *NS* probe hybridized poorly with these small RNAs, which were spliced at the D1 donor and thus contained a small exon (~57 nts), due to sequence variation between V9 and A6.

Combining the results obtained from RNase protection assay and Northern blot analysis enabled us to establish the transcription maps for V9 and A6, respectively, as shown in Fig. 3. In general, alternative processing of the V9 and A6 RNAs from transfected COS-7 cells generated different RNA species that are required to produce the non-structural proteins, i.e. NS1, 8 kDa and 10 kDa, and the structural proteins, VP1 and VP2. In the case of A6 RNA processing, the failure of splicing at the A1-2 acceptor does not prevent generation of sufficient mRNA species encoding for these viral proteins. The R1′, R2′ and R3′ mRNAs of the V9 RNA and the R1′ and R2′ mRNAs of the A6 RNA were polyadenylated at the (pA)p2 site and did not appear clearly on Northern blots, indicating that they are likely minor transcripts. In genotype-1 B19V, RNA polyadenylated at the (pA)p2 accounts for only 10% of the RNA that is internally polyadenylated (Yoto et al., 2006). The 4.7 kb R0 mRNA present on maps of V9 and A6 is the full-length transcript that reads through the (pA)p sites. It was detected in genotype-1 RNA from transfected cells (Liu et al., 2004), but not in genotype-1 RNA from virus-infected cells (Ozawa et al., 1987). Since the genotype-1 RNA profile generated in COS-7 cells following transfection with a replication-competent construct is similar to that following infection with genotype-1 virus (St et al., 1991; Yoto et al., 2006; Guan et al., 2008), we believe that the transcription profiles of A6 and V9 during virus infection are similar to those observed in transfected cells.

In B19V-permissive UT7/Epo-S1 cells, B19V genotype-1 ITRs support replication of the incomplete V9 genome, which produces infectious progeny virus, but not of the A6 genome

The terminal repeats of both genotype-2 and genotype-3 have not been characterized; therefore, we next examined whether the prototype-1 terminal repeats can support replication of the A6 or the V9 incomplete genome in UT7/Epo-S1 cells. To this end, we constructed chimeric genomes of B19VITR-V9 and B19VITR-A6, as diagramed in Fig. 4A, by inserting the P6-driven NS1- and Cap-encoding region (*NSCap*) of the two variants into vectors bearing the B19V ITRs derived from an infectious clone of genotype-1, pB19-M20 (Zhi et al., 2004). Excised B19V DNAs were transfected into UT7/Epo-S1 cells and low molecular-weight DNA was extracted for Southern blot analysis. B19V DNA replication can be identified by the presence of a *Dpn*I-digestion-resistant DNA band. As shown in Fig. 4B, the prototypic ITRs supported replication of the V9 *NSCap*, but not the A6 *NSCap* (Fig. 4B, lanes 8 and 10, respectively), suggesting that the A6 NS1 protein may contain mutations that prevent replication of the genotype-1 ITRs-containing A6 genome. The positive control (the infectious genotype-1 DNA, M20) generated significant quantities of *Dpn*I-resistant DNA (Fig. 4B, lane 4). In contrast, the negative control [the NS1-knock-out mutant, M20NS1(−)], did not produce a *Dpn*I-resistant band (Fig. 4B, lane 6). NS1 expression was confirmed in cells transfected with the M20, B19VITR-V9 and B19VITR-A6 DNAs, but not in M20NS1(−)-transfected cells (data not shown). Based on these findings, we predict that the ITR structure of the A6 variant must differ from that of the prototypic ITR.

We next set out to determine whether transfecting UT7/Epo-S1 cells with B19VITR-V9 or B19VITR-A6 leads the production of infectious progeny virus. To this end, we transfected UT7/Epo-S1 with B19VITR-V9 or B19VITR-A6 and used lysates of these cells to infect B19V-permissive *ex vivo*-expanded $CD36^+$ erythroid progenitor cells ($CD36^+$ EPCs) (Wong et al., 2008; Guan et al., 2008). Lysates generated from UT7/Epo-S1 cells transfected with M20 DNA and M20NS(−) served as a positive and a negative control, respectively. The production of progeny virus was assayed by the infectivity of $CD36^+$ EPCs, and quantified by reverse-transcription (RT)-real time PCR analysis of spliced VP2 and 11-/10-kDa viral mRNAs produced in infected $CD36^+$ EPCs. The infectivity of the progeny virus obtained from lysates of B19VITR-V9-transfected UT7/Epo-S1 cells was nearly equivalent to that of virus in lysates of M20-transfected (positive control) cells. In contrast, infectivity of the progeny virus from lysates from B19VITR-A6-transfected UT7/Epo-S1 cells and M20NS(−) (negative control) -transfected cells, could not be detected (Fig. 4C). These results further confirmed that, in UT7/Epo-S1 cells, replication competence and progeny virus production of the V9 genome is supported by the genotype-1 B19V ITRs, but that is not the case for the A6 genome.

The V9 and A6 NS1 proteins are potent inducers of apoptosis in UT7/Epo-S1 cells

B19V infection induces cell death through an apoptotic pathway, in both primary erythroid cells and B19V-permissive cell lines (Sol et al., 1999; Moffatt et al., 1998). This cell death has been attributed to the NS1 protein. Apoptosis has been reported to be induced in the NS1-expressing UT7/Epo-S1 as well as in NS1-transfected cells (Sol et al., 1999; Moffatt et al., 1998; Poole et al., 2004). Given that the A6 and V9 NS1 proteins diverge approximately 6.0 from that of the genotype-1, we decided to examine the pro-apoptotic nature of these two novel NS1 proteins. After initiating apoptosis, cells translocate the membrane phosphatidylserine from the inner face of the plasma membrane to the cell surface, and this event can be easily detected by staining with a FITC-conjugated AnnexinV protein. AnnexinV staining requires the use of living cells. To sort NS1-expressing cells, we transfected GFP-fused V9 and A6 NS1constructs into UT7/Epo-S1 cells. Two days after transfection, cells then were stained alive with AnnexinV and PI and were analyzed by flow cytometry. GFP-fused genotype-1 NS1 and GFP alone were used as positive and negative controls, respectively. Our results showed that both NS1 proteins of the A6 and V9 variants behaved much like the genotype-1 B19V NS1,

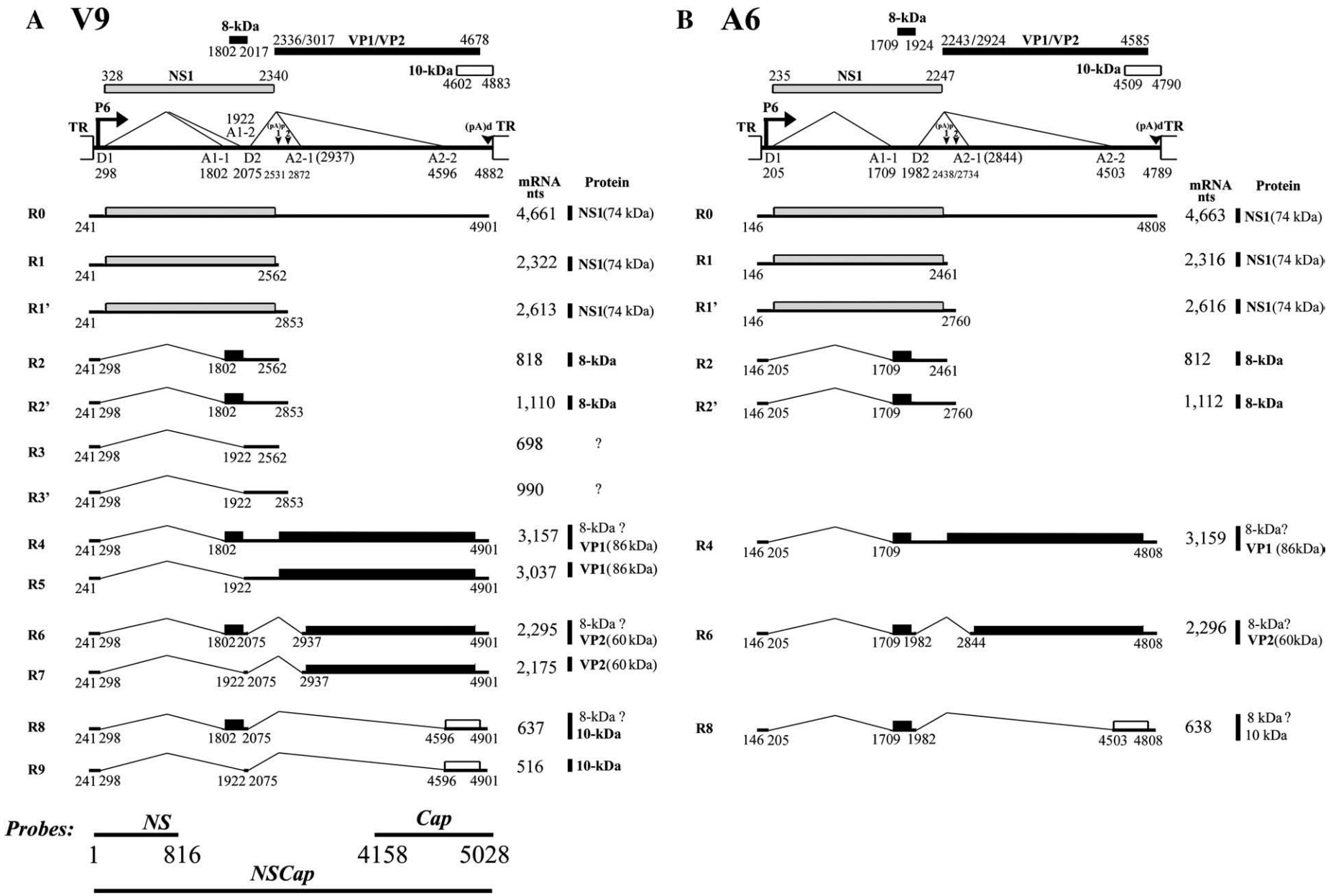

Fig. 3. Transcription maps of V9 and A6. The V9 and A6 genomes in panels A and B, respectively, are shown to scale with transcription landmarks confirmed by RPA [i.e. the P6 promoter, the splice donors (D), and acceptors (A) sties, the (pA)p and the (pA)d]. All of the RNA species detected are diagrammed, with their sizes in absence of the polyA tail indicated. The ORFs that each encodes [with reference to those shown in the B19V map (Ozawa et al., 1987; Guan et al., 2008)] are also diagramed, and the predicted sizes (kDa) of the translated proteins are indicated.

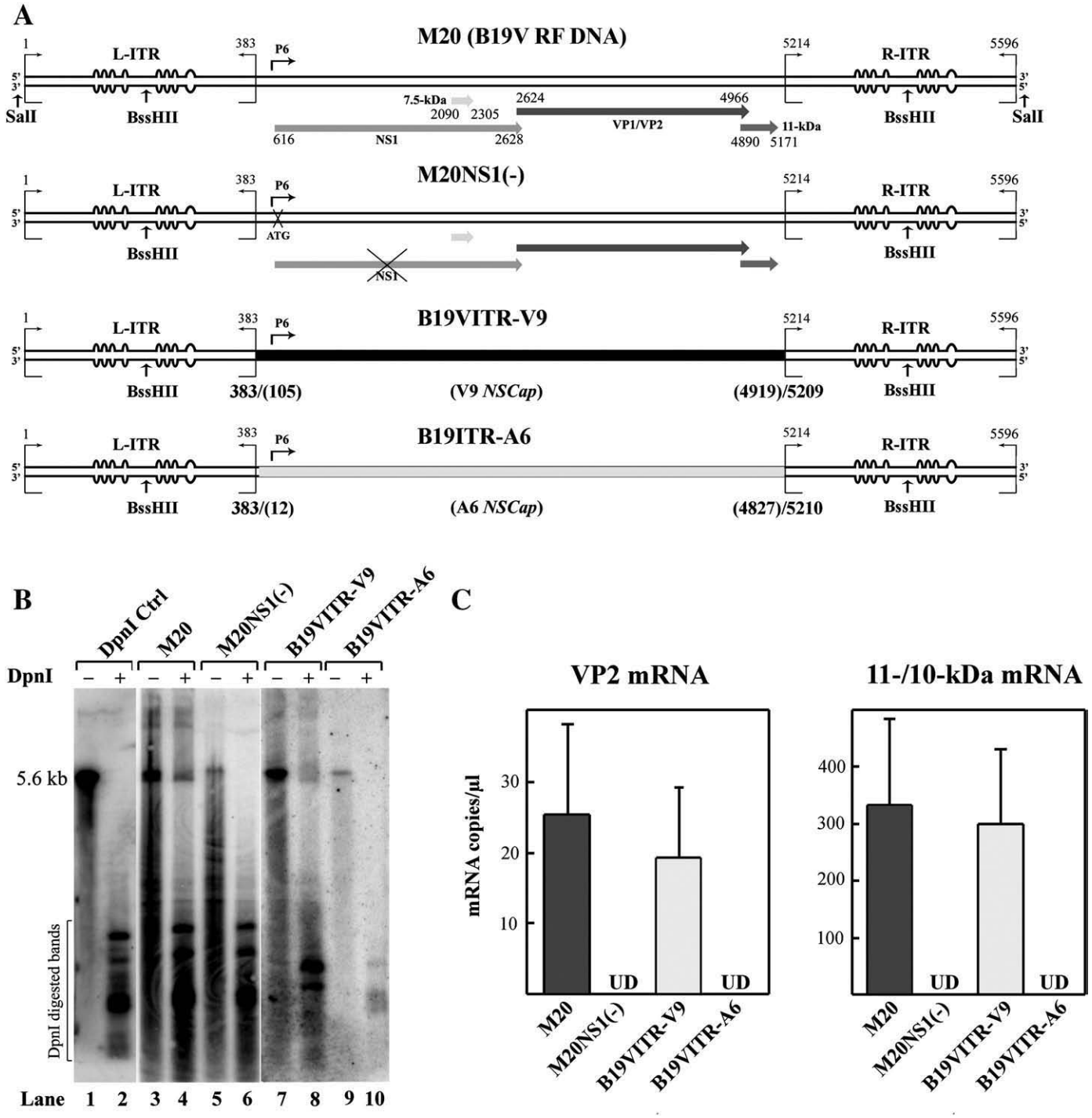

Fig. 4. Replication of the V9 and A6 *NSCap* genomes in the presence of genotype-1 ITRs. (A) Schematic diagrams of B19V DNAs. B19V DNA M20 is the duplex replicative form (RF) of the genotype-1 genome, which is able to replicate and produce progeny virus in B19V-permissive cells (Zhi et al., 2004). The bubbles within each ITR reflect potential inter-strand folding. The position of the P6 promoter, as well as those of the ORFs for the five B19V proteins, is also indicated. The prototype B19V ITRs were fused to both ends of the V9 and A6 genomes, at nucleotide numbers shown as ITR nucleotide number/(V9 or A6 nucleotide number), under the diagram of each chimeric construct (B19VITR-V9 or B19VITR-A6). *Bss*HII sites were used to clone the V9 or A6 genome into the prototype B19V ITRs, as described in the Materials and methods section. (B) Southern blot analysis. Hirt DNA isolated from excised B19VITR-V9- or B19VITR-A6-transfected UT7/Epo-S1 cells two days post-transfection was digested with *Eco*RI and *Dpn*I which are indicated as *Dpn*I (−) and *Dpn*I+ samples, respectively, and these samples were used in Southern blot analysis. Hirt DNA samples isolated from B19V M20- and M20NS1(−)-transfected UT7/Epo-S1cells were used as positive and negative controls, respectively, of B19V DNA replication. The blot was hybridized to the B19V *NSCap* DNA probe (Guan et al., 2008). *Eco*RI-digested and *Dpn*I-digested M20 DNA (6 ng) were run in lane 1 and lane 2, respectively, and were used as a control of *Dpn*I digestion and a DNA size maker. (C) Quantification of progeny virus production. UT7/Epo-S1 cells were transfected with four B19V DNAs, as shown in panel A. Cell lysates prepared at three days post-transfection were used to infect $CD36^+$ EPCs, and the infectivity of these cell lysates was quantified by a RT-real-time-PCR strategy that detected specifically the VP2 and 11-/10-kDa mRNAs in the $CD36^+$ EPCs lysates. In each sample, the absolute number of mRNA copies was normalized to the level of β-actin mRNA (10^4 copies per μl). Results shown represent the average and standard deviation for data from at least three independent experiments. "UD" denotes undetectable.

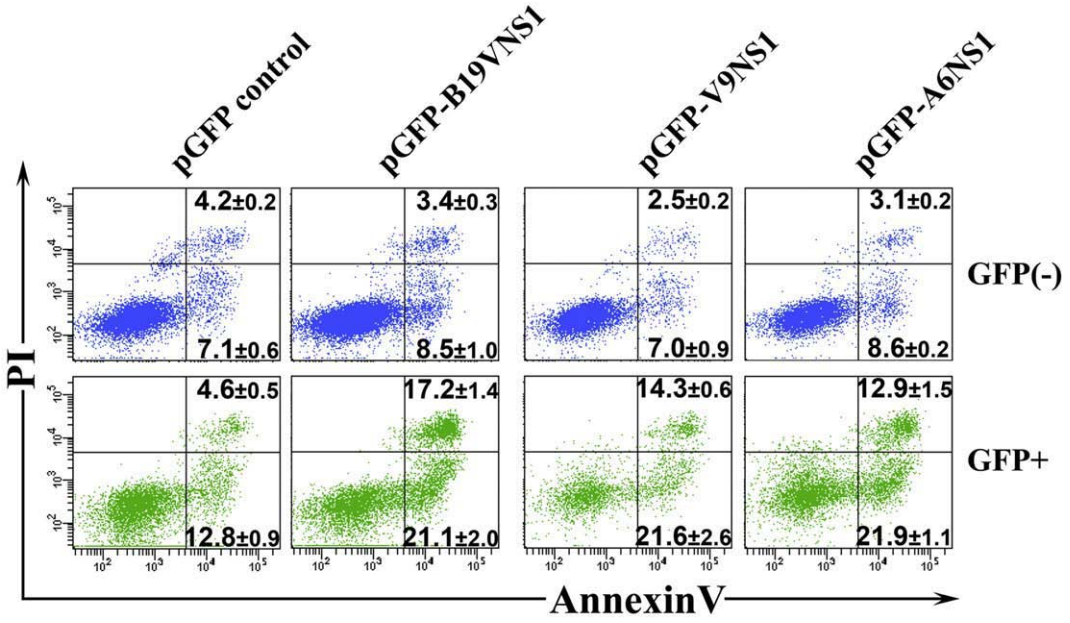

Fig. 5. Transfection of V9 and A6 NS1 induces apoptosis in B19V-permissive cells. UT7/Epo-S1 cells were transfected with pGFP (as negative control), pGFP-B19VNS1 (positive control), pGFP-V9NS1 and pGFP-A6NS1. Cells were double-stained with AnnexinV and propidium iodide (PI) at two days post-transfection, and were then subjected to flow cytometry. Both GFP-negative [GFP(−)] and GFP-positive (GFP+) cell populations were gated to plot cells by PI staining vs. AnnexinV staining. A representative experiment of three is shown. The average percentages with standard deviation of the AnnexinV+/PI+ and AnnexinV+/PI− populations are shown in the upper right and lower right quadrants, respectively.

inducing a significant percentage of the GFP-positive (GFP+) cells in the population of transfected cells to also become AnnexinV-positive compared with the GFP control (Fig. 5). However, in GFP negative [GFP(−)] cells, the population of AnnexinV+ among those transfected with the genotype-1, A6, and V9 GFP-NS1 constructs did not differ significantly from that of the GFP transfection control. More specifically, in the GFP+ cell population, transfection of the genotype-1, V9 and A6 GFP-NS1 constructs induced AnnexinV+/PI- populations of 21.1%, 22.6% and 22.9%, respectively (cells at early stages of apoptosis) (Fig. 5). In the same population, genotype-1, V9 and A6 GFP-NS1 induced an AnnexinV+/PI+ population of 17.2%, 14.3% and 12.9%, respectively (cells at late stages of apoptosis) (Fig. 5). The GFP control only induced an AnnexinV+/PI− and an AnnexinV+/PI+ populations of 12.8% and 4.6%, respectively (Fig. 5). We thus conclude that both NS1 proteins of the genotypes 2 and 3 have a potency similar to that of the prototype NS1 to induce apoptosis in UT7/Epo-S1 cells.

Discussion

Recently, human parvovirus B19V has been described to diverge genetically (Hokynar et al., 2007). However, serological studies of the three genotypes of B19V confirmed that they belong to one serotype (Ekman et al., 2007); and all the three genotypes show a tropism for erythroid cells (Hokynar et al., 2007). Since the transcription profile of prototype B19V generated by transfecting COS-7 cells is similar to that during virus infection of B19V-permissive cells (Ozawa et al., 1987; Beard et al., 1989; Liu et al., 2004; Yoto et al., 2006), we believe that the transcriptional profiles of V9 and A6 variants presented in this study resemble those during virus infection. A unique feature we have identified is that the genotype-2 A6 variant used only one splice acceptor to remove the first intron. However, the overall RNA profile of the genotype-3 V9 variant is the similar as that of the prototype B19V.

Prototype B19V replicates exclusively in erythroid progenitors of human bone marrow, and produces extraordinarily high virus yields in blood during the early phase of infection (Anderson et al., 1985; Enders et al., 2006; Ozawa et al., 1986). In contrast, high-titers of genotype-2 and genotype-3 are rarely identified (Blumel et al., 2005; Liefeldt et al., 2005; Nguyen et al., 1999, 2002; Servant et al., 2002). More importantly, the genotype-2 variant often persistently presents in skin; and genotype-3 has been suggested to have remained absent from wide circulation in Europe (Norja et al., 2006). In the current study, we have shown that the genotype-2 A6 variant uses only the first acceptor to remove the first intron, and therefore fails to produce the corresponding R5, R7 and R9 mRNAs (Fig. 3B). Although the R4, R6 and R8 mRNAs encode VP1, VP2 and 10 kDa, respectively, all three are di-cistronic and in them, the 8-kDa ORF is located upstream of the VP1/VP2 ORF and the 10-kDa ORF, respectively. It is thus possible that these di-cistronic mRNAs reduce the translation efficiency of VP1/VP2 and 10 kDa. In addition, the inactive A1-2 acceptor site could decrease the overall number of RNAs spliced at the D2 donor and, in turn, reduces the levels of protein expression during active virus replication. Thus, we hypothesize that the inactive A1-2 acceptor is probably a disadvantage for the processing of A6 virus mRNAs as well as a disadvantage for protein translation, which could possibly maintain virus production at a low level.

Sequence alignments among members of all three genotypes (nt 2139-2241 with respect to the prototype B19V J35 isolate, Genbank accession no.: AY386330) showed that only four variations present in the A1-2 acceptor region. Between V9 and A6, these nucleotides have only one difference, an A versus a G at nt 2179. Interestingly, the position of this nucleotide suggests that it could be the branch point for the A1-2 acceptor. However, mutation of the G to A in A6 genome did not rescue splicing at the A1-2 site (data not shown), suggesting that efficient splicing at the A1-2 site may require an exon and/or intron splicing enhancer. In fact, the three genotypes vary by approximately 12% in the region spanning the D2 donor (nt 2305-2581), which supports that variations in the potential splicing enhancers may affect splicing at the A1-2 acceptor site. We realized that the conclusion that the genotype-2 A6 used only one splice acceptor to remove the first intron was drawn only from results obtained by transfection of the cloned genome of A6 variant. However, an A6 mutant that bears an A mutation at nt 2180, which reverts to an identical sequence from nt 1800 to nt 2500 to that of the

Lali variant (Hokynar et al., 2002), did not rescue splicing at the A1-2 (data not shown). Further investigation into whether the A1-2 acceptor is used with genomes of other genotype-2 and their viruses, such as the IM-81 (Blumel et al., 2005), is required to demonstrate the biological importance of the inactive A1-2 acceptor.

The NS1 proteins of the three genotypes diverge significantly. The genotype-2 LaLi and genotype-3 V9 variants diverge nearly 13% from in the prototype B19V isolate within the NS1-encoding sequence (Hokynar et al., 2002). On the protein level, however, the LaLi, A6 and V9 variants are only 6.0% divergent from the B19V prototype. The B19V NS1 protein is a multifunctional protein. Parvovirus NS1 contains a DNA binding domain at its N-terminus, the conserved motifs for single-strand nicking activity and an ATP/helicase domain at the center, and a transcription activation domain at the C-terminus (Cotmore and Tattersall, 2006). The genotype-1 NS1 has been found to enhance equally on promoters of all three genotypes (Ekman et al., 2007). We have shown in this study that the genotype-2 A6 NS1 does not support replication of the genotype-1 ITR-based A6-*NSCap* genome (Fig. 4), suggesting that the 6% divergence either is sufficient to alter the specific binding of the A6 NS1 to the genotype-1 ITR, or to reduce the nicking activity at the terminal resolution site. Interestingly, in a similar genotype-1 ITR-based V9-*NSCap* genome, the V9 NS1 supported not only genotype-1 ITR-dependent replication, but also progeny virus production in UT7/Epo-S1 cells. Thus, the V9 NS1 is fully functional with respect to enabling replication of the B19VITR-V9 genome, as well as synthesis of the single-stranded DNA genome and its packaging. Therefore, we have shown, for the first time, that the divergent B19V NS1 proteins have genotype-specific activity in DNA replication. We hypothesize that the ITR structure of the A6 variant must differ from that of the genotype-1. Whether the NS1 of other genotype-2 variants is similar to the A6 NS1, and whether genotype-2 variants share a common ITR structure, require further investigation.

Our results also have confirmed that both the A6 and V9 NS1 proteins possess a similar potency in inducing apoptosis in B19V-permissive cells, indicating that the NS1 proteins of B19V genotypes 2 and 3 have the same function in the pathogenesis of virus infection as the prototype NS1. The prototypic NS1-induced cytotoxicity and apoptosis of infected erythroid progenitors cause the disease outcomes characteristic of B19V infection (Brown and Young, 1997; Moffatt et al., 1998; Sol et al., 1999).

Materials and methods

Cells

COS-7 cells (CRL-1651; ATCC) were maintained in Dulbecco's modified Eagle's medium (DMEM) with 10% fetal calf serum (FCS) at 37 °C in 5% CO_2. UT7/Epo-S1 cells were cultured in DMEM with 10% FCS and 2 units/ml of Epo [Procrit (Epoetin Alfa), Centocor Ortho Biotech Inc., Horsham, PA] at 37 °C in 5% CO_2. The process of generating of primary human $CD36^+$ erythroid progenitor cells ($CD36^+$ EPCs) has been described elsewhere (Guan et al., 2008; Wong et al., 2008).

Transfection

Per 60-mm dish, 2 μg of DNA were transfected into COS-7 cells, using Lipofectamine and Plus reagents (Invitrogen) as previously described (Qiu and Pintel, 2002). UT7/Epo-S1 cells were transfected with 2 μg of DNA per 2×10^6 cells using a universal reagent (DNAproject, WA) and program X005 using the Nucleofector (Lonza, MD).

Plasmid construction

pC1V9 and pC1A6 plasmids

The original A6 plasmid, a pCR-Blunt II TOPO (Invitrogen) vector into which the full-length coding sequence of A6 (4844 bp) without the 3′- and 5′-ITRs (Genbank accession no.: AY064475) had been cloned, was a gift from Dr. Kevin Brown. Plasmid pC1A6 was constructed by replacing the B19V *NSCap* gene with the A6 sequence of nt 1-4844 in pC1NS1(−) (Yoto et al., 2006). The pC1 backbone was constructed by removing the CMV-GFP expression cassette (nt 8-1477) from pEGFP-C1 (Clontech). A SV40-ori is included in pC1.

The V9-C22 plasmid, consisting of the entire V9 genome except the 3′- and 5′-ITRs (5028 bp, Genbank accession no.: AJ249437) was obtained from Collection National deCulture de Microorganisms (Institute Pasteur, Paris, France: CNCM1-2066) as a transferred material. pC1V9 was constructed by replacing the B19V *NSCap* gene with the V9 sequence encompassing nt 1-5028 in pC1NS1(−).

pB19VITR-V9 and pB19VITR-A6 plasmids

All the nucleotide numbers of the geneotype-1 B19V refer to the J35 isolate (Genbank accession no.: AY386330). To insert the A6 *NSCap* gene into the J35-ITRs from pM20 (an infectious clone of B19), we first modified the pN8 (Zhi et al., 2004) to contain the B19V sequence of nt 182-5412, including two half-ITRs with a *Bss*HII site, which was named pBssH-N8. Then, the B19V sequences of nt 383-5209 and nt 383-5210 on pBssH-N8 were replaced with the corresponding V9 sequence (nt 105-4919) and A6 sequence (nt 12-4827), respectively, which resulted in the plasmids pBssH-V9 and pBssH-A6. The *Bss*HII-digested large fragments of pBssH-V9 and pBssH-A6 were inserted into *Bss*HII-digested pM20, which resulted in the final plasmids pB19VITR-V9 and pB19VITR-A6, respectively. A schematic diagram of the excised DNAs of B19VITR-A6 and B19VITR-V9 is shown in Fig. 4A.

GFP-fused NS1 constructs

The NS1 ORFs of V9 (nt 328-2340), A6 (nt 235-2247) and B19V (nt 616-2628) were inserted into *Bam*HI–*Xho*I digested pcDNAGFP vector, respectively, to construct the pGFP-V9NS1, pGFP-A6NS1 and pGFP-B19VNS1, respectively. The pcDNA-GFP was made by inserting the GFP-coding sequence into the *Hin*dIII/*Bam*HI digested pcDNA3 (Invitrogen).

Clones used to generate probes for RNase protection

To map the transcription units of V9 and A6, we used probes V9 (A6) P1, P2, P3, P4 and P5. These probes were constructed by cloning the following regions of V9 (A6) into *Bam*HI–*Hin*dIII digested pGEM3Z (Promega): nt 193–432 (100–340) [V9 (A6) P1], nt 1710–2272 (1620–2180) [V9 (A6) P2], nt 2430–3095 (2338–3005) [V9 (A6) P3], nt 4433–4675 (4339–4582) [V9 (A6) P4] and nt 4712–4941 (4619–4844) [V9 (A6) P5].

RNA isolation, RNase protection and Northern blot analysis

Total RNA was isolated from transfected cells two days post transfection using TRIZOL reagent (Invitrogen).

An RNase protection assay was performed essentially as previously described (Naeger et al., 1992; Schoborg and Pintel, 1991). Probes were generated from *Bam*HI-digested templates by *in vitro* transcription with Sp6 polymerase using the MAXIscript® kit (Ambion) and following the manufacture's instruction. RNA hybridizations for RNase protection were done in the presence of a substantial excess of probe, and signals were quantified with the Storm 856 phosphor imager and Image Quant TL software v2005 (GE Healthcare). Relative molar ratios of individual RNA species were determined after adjusting for the number of ^{32}P-labeled uridines (U) in each protected fragment as previously described (Schoborg and Pintel, 1991).

Northern blot analyses were performed as previously described (Pintel et al., 1983; Qiu et al., 2002), using total RNA samples and ^{32}P-labeled DNA probes as indicated. All Northern probes were digested from corresponding plasmids and are diagramed in Fig. 3.

Southern blot analysis

At two days after transfection, cells were collected and washed twice with phosphate-buffered saline. Isolation of low molecular-weight DNA (Hirt DNA) and Southern blotting were performed essentially as described previously (Guan et al., 2008). Blots were hybridized with the V9 *NSCap* probe (nt 1-5028) (Fig. 3), and signals were developed by exposing the blots to X-ray film.

Virus generation and infection

Transfected UT7/Epo-S1 cells were harvested three days after transfection. After the cells were frozen and thawed three times, supernatant was collected. 200 μl of the supernatant were incubated with 2×10^5 of $CD36^+$ EPCs with a slow rotation, at 4 °C for 1.5 h. Infected cells were pelted by low-speed centrifugation, and were cultured at a concentration of 2×10^5 cells/ml at 37 °C with 5% CO_2. At 3 days postinfection, mRNA was directly isolated from the cells, using the TurboCapture 8 mRNA kit (Qiagen) according to the manufacturer's instructions.

Reverse transcription (RT) and real time-PCR

Isolated mRNA was reverse-transcribed to cDNA using random hexamers (Promega) and MMLV-RT (Invitrogen), following the manufacturer's instructions. cDNA copy number was determined by real-time PCR as described previously (Guan et al., 2008, 2009), using the TaqMan universal PCR master mix (Takara).

The forward and reverse primers and probe used in real-time PCR for cDNAs converted from the respective genotype-1 VP2 and 11 kDa mRNAs were described previously (Guan et al., 2009). The probes used for cDNAs converted from A6 VP2 and 10-kDa mRNAs were the same as those used for prototype B19V, respectively, and the forward and reverse primers used were as follows: for VP2 mRNA: 5′-GACCAGTTCAGGAGAATCAT-3′ (nt 1875–1894), 5′-TTCTGAGGCGTTGTATGC-3′ (nt 2911–2894); for 10-kDa mRNA: 5′-GAAGCCTTT TACACTCCACTTG-3′ (nt 1942–1963), 5′-TGGCAGTCCACAATTCTTCAGG-3′ (nt 4565–4544). The probe used for cDNAs converted from V9 VP2 mRNA was the same for prototype VP2 mRNA, and the probe used for cDNA converted from V9 10-kDa mRNA were as the following: 5′FAM-CGATCAGTTTCGTGAACT/CTACAGATGGA-3′BHQ (D2/A2-2). The forward and reverse primers used for cDNAs converted from V9 VP2 and 11 kDa mRNAs were as follows: for VP2 mRNA: 5′-5′-GACCAGTTCAGGAGAATCAT-3′ (nt 1968–1988)-3′, 5′-TTCTGAGGCGTTGTACGC-3′ (nt 3004–2987); for 10-kDa mRNA: 5′-GAAGCTTTTTACACGCTT G-3′ (nt 2035–2056), 5′-TGGCAGTCCACAATTCTTCAG G-3′ (nt 4568–4637).

All the splice donor (D2) and acceptor (A2-1 and A2-2) sites for prototype B19V were described as previously (Guan et al., 2008), and those for A6 and V9 are described in Fig. 3.

cDNA copies of β-actin mRNA were quantified using the forward and reverse primers and probe as previously reported using JOE-labeled TaqMan probe (Kammula et al., 1999). Standard curves for β-actin, VP2 and 11-/10-kDa cDNAs were generated from serial dilutions of a β-actin cDNA plasmid (Wong et al., 2008) and the B19V, V9 and A6 VP2 cDNA and 11-/10-kDa cDNA plasmids. The copy numbers of all B19V mRNAs are presented as copies per μl of the cDNA reaction mixture, and were normalized with respect to the copy number of the β-actin mRNA produced in the same reaction.

Flow cytometry analysis

Cells were double-stained live with Cy5-conjugated AnnexinV (BD Biosciences) and Propidium Iodide (PI, Sigma) in order to detect apoptotic cells. Staining was carried out according to the manufacturer's instructions (BD Biosciences). All samples were analyzed on the three-laser flow cytometer (LSR II, BD Biosciences) at the Flow Cytometry Core of the University Kansas Medical Center. Flow cytometry data were analyzed using FACS DIVA software (BD Biosciences).

Acknowledgments

This work was supported by PHS grant RO1 AI070723 from NIAID and grant P20 RR016443 from the NCRR COBRE program. We thank Dr. Kevin Brown for providing valuable reagents.

References

Allander, T., Tammi, M.T., Eriksson, M., Bjerkner, A., Tiveljung-Lindell, A., Andersson, B., 2005. Cloning of a human parvovirus by molecular screening of respiratory tract samples. Proc. Natl. Acad. Sci. U. S. A. 102 (36), 12891–12896.
Anderson, M.J., Jones, S.E., Minson, A.C., 1985. Diagnosis of human parvovirus infection by dot–blot hybridization using cloned viral DNA. J. Med. Virol. 15 (2), 163–172.
Beard, C., St, A.J., Astell, C.R., 1989. Transient expression of B19 parvovirus gene products in COS-7 cells transfected with B19-SV40 hybrid vectors. Virology 172 (2), 659–664.
Blumel, J., Eis-Hubinger, A.M., Stuhler, A., Bonsch, C., Gessner, M., Lower, J., 2005. Characterization of Parvovirus B19 genotype 2 in KU812Ep6 cells. J. Virol. 79 (22), 14197–14206.
Brown, K.E., Young, N., 1997. Human parvovirus B19: Pathogenesis of disease. In: Anderson, L.J., Young, N. (Eds.), Human parvovirus B19. Karger, Basel, Switzerland, pp. 105–119.
Candotti, D., Etiz, N., Parsyan, A., Allain, J.P., 2004. Identification and characterization of persistent human erythrovirus infection in blood donor samples. J. Virol. 78 (22), 12169–12178.
Cotmore, S.F., Tattersall, P., 2006. In: Kerr, J., Cotmore, S.F., Bloom, M.E., Linden, R.M., Parrish, C.R. (Eds.), A rolling-haipin strategy: basic mechanisms of DNA replication in the parvoviruses. In Parvoviruses. Hoddler Arond, London, pp. 171–181.
Ekman, A., Hokynar, K., Kakkola, L., Kantola, K., Hedman, L., Bonden, H., Gessner, M., Aberham, C., Norja, P., Miettinen, S., Hedman, K., Soderlund-Venermo, M., 2007. Biological and immunological relations among human parvovirus B19 genotypes 1 to 3. J. Virol. 81 (13), 6927–6935.
Enders, M., Schalasta, G., Baisch, C., Weidner, A., Pukkila, L., Kaikkonen, L., Lankinen, H., Hedman, L., Soderlund-Venermo, M., Hedman, K., 2006. Human parvovirus B19 infection during pregnancy—value of modern molecular and serological diagnostics. J. Clin. Virol. 35 (4), 400–406.
Guan, W., Cheng, F., Yoto, Y., Kleiboeker, S., Wong, S., Zhi, N., Pintel, D.J., Qiu, J., 2008. Block to the production of full-length B19 virus transcripts by internal polyadenylation is overcome by replication of the viral genome. J. Virol. 82 (20), 9951–9963.
Guan, W., Wong, S., Zhi, N., Qiu, J., 2009. The genome of human parvovirus B19 virus can replicate in non-permissive cells with the help of adenovirus genes and produces infectious virus. J. Virol. 83 (18), 9541–9553.
Hokynar, K., Soderlund-Venermo, M., Pesonen, M., Ranki, A., Kiviluoto, O., Partio, E.K., Hedman, K., 2002. A new parvovirus genotype persistent in human skin. Virology 302 (2), 224–228.
Hokynar, K., Norja, P., Hedman, K., Soderlund-Venermo, M., 2007. Tissue persistence and prevalence of B19 virus types 1–3. Future Virol. 2 (4), 377–388.
Kammula, U.S., Lee, K.H., Riker, A.I., Wang, E., Ohnmacht, G.A., Rosenberg, S.A., Marincola, F.M., 1999. Functional analysis of antigen-specific T lymphocytes by serial measurement of gene expression in peripheral blood mononuclear cells and tumor specimens. J. Immunol. 163 (12), 6867–6875.
Liefeldt, L., Plentz, A., Klempa, B., Kershaw, O., Endres, A.S., Raab, U., Neumayer, H.H., Meisel, H., Modrow, S., 2005. Recurrent high level parvovirus B19/genotype 2 viremia in a renal transplant recipient analyzed by real-time PCR for simultaneous detection of genotypes 1 to 3. J. Med. Virol. 75 (1), 161–169.
Liu, Z., Qiu, J., Cheng, F., Chu, Y., Yoto, Y., O'Sullivan, M.G., Brown, K.E., Pintel, D.J., 2004. Comparison of the transcription profile of simian parvovirus with that of the human erythrovirus B19 reveals a number of unique features. J. Virol. 78 (23), 12929–12939.
Moffatt, S., Yaegashi, N., Tada, K., Tanaka, N., Sugamura, K., 1998. Human parvovirus B19 nonstructural (NS1) protein induces apoptosis in erythroid lineage cells. J. Virol. 72 (4), 3018–3028.
Naeger, L.K., Schoborg, R.V., Zhao, Q., Tullis, G.E., Pintel, D.J., 1992. Nonsense mutations inhibit splicing of MVM RNA in cis when they interrupt the reading frame of either exon of the final spliced product. Genes Dev. 6 (6), 1107–1119.
Nguyen, Q.T., Sifer, C., Schneider, V., Allaume, X., Servant, A., Bernaudin, F., Auguste, V., Garbarg-Chenon, A., 1999. Novel human erythrovirus associated with transient aplastic anemia. J. Clin. Microbiol. 37 (8), 2483–2487.
Nguyen, Q.T., Wong, S., Heegaard, E.D., Brown, K.E., 2002. Identification and characterization of a second novel human erythrovirus variant, A6. Virology 301 (2), 374–380.
Norja, P., Hokynar, K., Aaltonen, L.M., Chen, R., Ranki, A., Partio, E.K., Kiviluoto, O., Davidkin, I., Leivo, T., Eis-Hubinger, A.M., Schneider, B., Fischer, H.P., Tolba, R., Vapalahti, O., Vaheri, A., Soderlund-Venermo, M., Hedman, K., 2006. Bioportfolio: lifelong persistence of variant and prototypic erythrovirus DNA genomes in human tissue. Proc. Natl. Acad. Sci. U. S. A. 103 (19), 7450–7453.
Ozawa, K., Kurtzman, G., Young, N., 1986. Replication of the B19 parvovirus in human bone marrow cell cultures. Science 233 (4766), 883–886.

Ozawa, K., Ayub, J., Hao, Y.S., Kurtzman, G., Shimada, T., Young, N., 1987. Novel transcription map for the B19 (human) pathogenic parvovirus. J. Virol. 61 (8), 2395–2406.

Pintel, D., Dadachanji, D., Astell, C.R., Ward, D.C., 1983. The genome of minute virus of mice, an autonomous parvovirus, encodes two overlapping transcription units. Nucleic Acids Res. 11 (4), 1019–1038.

Poole, B.D., Karetnyi, Y.V., Naides, S.J., 2004. Parvovirus B19-induced apoptosis of hepatocytes. J. Virol. 78 (14), 7775–7783.

Qiu, J., Pintel, D.J., 2002. The adeno-associated virus type 2 Rep protein regulates RNA processing via interaction with the transcription template. Mol. Cell. Biol. 22 (11), 3639–3652.

Qiu, J., Nayak, R., Tullis, G.E., Pintel, D.J., 2002. Characterization of the transcription profile of adeno-associated virus type 5 reveals a number of unique features compared to previously characterized adeno-associated viruses. J. Virol. 76 (24), 12435–12447.

Sanabani, S., Neto, W.K., Pereira, J., Sabino, E.C., 2006. Sequence variability of human erythroviruses present in bone marrow of Brazilian patients with various parvovirus B19-related hematological symptoms. J. Clin. Microbiol. 44 (2), 604–606.

Schoborg, R.V., Pintel, D.J., 1991. Accumulation of MVM gene products is differentially regulated by transcription initiation, RNA processing and protein stability. Virology 181 (1), 22–34.

Servant, A., Laperche, S., Lallemand, F., Marinho, V., De Saint, M.G., Meritet, J.F., Garbarg-Chenon, A., 2002. Genetic diversity within human erythroviruses: identification of three genotypes. J. Virol. 76 (18), 9124–9134.

Sol, N., Le, J.J., Vassias, I., Freyssinier, J.M., Thomas, A., Prigent, A.F., Rudkin, B.B., Fichelson, S., Morinet, F., 1999. Possible interactions between the NS-1 protein and tumor necrosis factor alpha pathways in erythroid cell apoptosis induced by human parvovirus B19. J. Virol. 73 (10), 8762–8770.

Srivastava, A., Lu, L., 1988. Replication of B19 parvovirus in highly enriched hematopoietic progenitor cells from normal human bone marrow. J. Virol. 62 (8), 3059–3063.

St, A.J., Beard, C., Humphries, K., Astell, C.R., 1991. Analysis of splice junctions and in vitro and in vivo translation potential of the small, abundant B19 parvovirus RNAs. Virology 183 (1), 133–142.

Wong, S., Zhi, N., Filippone, C., Keyvanfar, K., Kajigaya, S., Brown, K.E., Young, N.S., 2008. Ex vivo-generated CD36+ erythroid progenitors are highly permissive to human parvovirus B19 replication. J. Virol. 82 (5), 2470–2476.

Yoto, Y., Qiu, J., Pintel, D.J., 2006. Identification and characterization of two internal cleavage and polyadenylation sites of parvovirus B19 RNA. J. Virol. 80 (3), 1604–1609.

Young, N.S., Brown, K.E., 2004. Parvovirus B19. N. Engl. J. Med. 350 (6), 586–597.

Zhi, N., Zadori, Z., Brown, K.E., Tijssen, P., 2004. Construction and sequencing of an infectious clone of the human parvovirus B19. Virology 318 (1), 142–152.